Viscoelastic Dynamics of Actin Filaments Coupled to Rotary F-ATPase: Angular Torque Profile of the Enzyme

Oliver Pänke, Dmitry A. Cherepanov, Karin Gumbiowski, Siegfried Engelbrecht, and Wolfgang Junge
Division of Biophysics, University of Osnabrück, D-49069 Osnabrück, Germany

ABSTRACT ATP synthase (F_OF_1) operates as two rotary motor/generators coupled by a common shaft. Both portions, F_1 and F_O, are rotary steppers. Their symmetries are mismatched (C_3 versus C_{10-14}). We used the curvature of fluorescent actin filaments, attached to the rotating **c**-ring, as a spring balance (flexural rigidity of $8 \cdot 10^{-26}$ Nm^2) to gauge the angular profile of the output torque at F_O during ATP hydrolysis by F_1 (see theoretical companion article (Cherepanov, D. A., and W. Junge, 2001. *Biophys. J.* 81:1234–1244.)). The large average output torque (50 ± 6 pN · nm) proved the absence of any slip. Variations of the torque were small, and the output free energy of the loaded enzyme decayed almost linearly over the angular reaction coordinate. Considering the threefold stepping and high activation barrier of the driving motor proper, the rather constant output torque implied a soft elastic power transmission between F_1 and F_O. It is considered as essential, not only for the robust operation of this ubiquitous enzyme under symmetry mismatch, but also for a high turnover rate of the two counteracting and stepping motor/generators.

INTRODUCTION

F_1F_O-ATP synthase is a twin rotary engine that drives ATP synthesis in its peripheral portion, F_1, at the expense of proton (sodium) flow through its membrane portion, F_O. These two functions are mechanically coupled by a common central shaft that rotates relative to an eccentric bearing (see Fig. 1 for an illustration). The "rotor" is composed from subunits $\varepsilon\gamma\mathbf{c}_{10\text{-}14?}$ and the "stator" from subunits $\mathbf{ab}_2\delta(\alpha\beta)_3$. There are three catalytic sites on F_1. They are equivalent in the time average, but structurally (Abrahams et al., 1994) and functionally (Weber and Senior, 1996) different at any moment. Their functional state rotates during turnover. The rotor portion of F_O is a ring of N identical copies of subunit **c**, so that the translocation of N ions has to be matched to the synthesis/hydrolysis of three molecules of ATP (for reviews see Junge et al., 1997; Boyer, 1997; Kinosita et al., 1998; Oster and Wang, 1999; Leslie et al., 1999; Dimroth, 2000)). The copy number, N, of subunit **c** is under contention. The enzyme can work with 12 copies in *Escherichia coli* (Jones and Fillingame, 1998), but ring constructs with different numbers have been reported based on x-ray crystal structure analysis (10, yeast; Stock et al., 1999) and atomic force microscopy (14, chloroplast; Seelert et al., 2000), (11, *Ilyobacter tartaricus*; Stahlberg et al., 2001).

Microvideography of fluorescent f-actin filaments that are attached to the rotor of the immobilized F_1 portion has been established as a powerful single-molecule approach to study the mechanical properties of this enzyme (Noji et al., 1997). In studies on isolated F_1 the average torque of the enzyme has been inferred from the average angular velocity of the long actin filament (see in particular Yasuda et al., 1998). Figures have ranged around 40 pN · nm. When sustained over an angular domain of $2\pi/3$ (the apparent angular progression per molecule of ATP hydrolyzed) this torque is equivalent to a free energy of 51 kJ/mol, considerably less than the assumed free energy of ATP hydrolysis in the cited experiments (72-87 kJ/mol, see Yasuda et al., 1998). Still, the rather moderate agreement has been claimed to prove almost 100% efficiency of this molecular machine (Wang and Oster, 1998; Kinosita, Jr., et al., 2000b).

The rate of ATP hydrolysis by isolated and load-free F_1 can range up to 300 s^{-1}, which is equivalent to 100 revolutions/s. Under these conditions of saturating ATP concentrations the three-stepped rotation of subunit γ has been recorded by polarized photobleaching absorption recovery with a single chromophore on subunit γ (Sabbert and Junge, 1997; Sabbert et al., 1997), by polarized fluorescence of such a probe (Häsler et al., 1998; Adachi et al., 2000), and recently by dark-field microscopy using a nano-gold particle as a probe on subunit γ (Yasuda et al., 2001). Additionally, at lower ATP concentrations (1 μM) Yasuda et al. resolved 90° and 30° substeps, which they attributed to ATP binding and ADP release, respectively (Yasuda et al., 2001). Three-stepped progression has also been observed using a micrometer-long actin filament on subunit γ; then, however, only at rate-limiting ATP concentrations (10 nM). They caused very low turnover rates (0.1 s^{-1}), thereby allowing the filament to relax from one into the next resting position (Yasuda et al., 1998). At saturating ATP concentrations (100 μM) no such stepping has been reported by monitoring rotating actin filaments. Assessments of the torque profile as function of the angular reaction coordinate have not yet been attempted. In the companion article (Cherepanov and Junge, 2001) we have theoretically studied the viscoelastic

Received for publication 15 February 2001 and in final form 6 June 2001.

Address reprint requests to Dr. Wolfgang Junge, Dept. of Biology and Chemistry, University of Osnabruck, Barbarastrasse 11, D-49076 Osnabruck, Germany. Tel.: 49-541-969-2872; Fax: 49-541-969-2870; E-mail: junge@biologie.uni-osnabrueck.de.

D. A. Cherepanov's permanent address is Franklin Institute of Electrochemistry, Moscow, Russia.

0006-3495/01/09/1220/14 $2.00

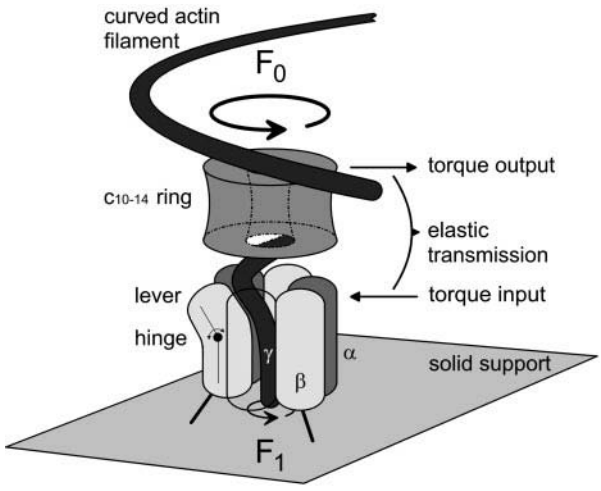

FIGURE 1 Schematic representation of the experimental setup, illustrating 1) the input torque generator, F_1, immobilized by three his-tags to a solid support; 2) the power transmission into the ring of subunits **c**, and 3) the actin filament, attached to the **c**-ring. Subunits δ, ε, **a**, **b**, and one copy of β were omitted for clarity and simplicity. The lever moving around a hinge on one copy of subunit β and pushing the convex side of γ symbolizes the site of torque input. The "elastic power transmission" is tentatively assigned to the following elements: the β lever, a stretch of γ, ε, and the **c**-ring. The site of torque output is at the interface between the **c**-ring and the actin filament. Because the functional coupling between subunits **a**, $\mathbf{b}_2$, and $\mathbf{c}_{10\text{-}14}$ with proton pumping was probably absent (see text) the stator did not contribute to elasticity in this experimental setup. The filament was curved under the influence of the torque provided by the enzyme and the counter-torque by its motion through the viscous medium and contacts with the surface of the solid support.

dynamics of rotating filaments. We arrived at two conclusions: 1) the rate of rotation of actin filaments of micrometer length is a poor indicator of the torque because of the filament's slow viscoelastic relaxation, and 2) the curvature of actin filaments, however, can be used to gauge the torque at any given angular position. In other words, the seeming disadvantage of the slow viscoelastic relaxation can be turned into a useful tool.

Following these technical lines we asked whether and to what extent the threefold stepping of ATP hydrolysis, which is established for load-free F_1, is elastically buffered in the loaded holoenzyme to match to the feasible 10- to 14-fold stepping of proton translocation in F_O. We took an actin filament on the **c**-ring as a model for the native load on F_O (powered by the ionmotive force) and asked for the output torque at the **c**-ring in relation to the stepped input torque delivered by the rotary drive in F_1. Fig. 1 illustrates the configuration of 1) the inner drive, 2) the assumed elastic transmission, 3) the **c**-ring, and attached to it 4) the actin filament as reporter-element, but also as the source of external load on the enzyme.

Cys-free *E. coli* F_OF_1 was immobilized on a solid support by three engineered his-tags, and an actin filament was attached to the **c**-ring through engineered strep-tags at the C-terminal end of subunit **c** (Pänke et al., 2000). Thereby we avoided possible pitfalls in the assignment of the attachment site that were discussed elsewhere (compare Tsunoda et al., 2000; Pänke et al., 2000). The fluorescent filaments were microvideographed as pioneered by Noji et al., 1997.

We found that the major resistance to rotary motion of the actin filaments was owed to the surface viscosity of the medium and to nonviscous interactions with the protein-doped solid support, but not by the viscous drag of the bulk fluid, as previously assumed (Yasuda et al., 1998). This result was corroborated by the analysis of filament bending fluctuations yielding the flexural rigidity about $8 \cdot 10^{-26}$ N $\cdot$ m^2. The magnitude of the output torque by curvature analysis was three times greater than determined in the common way by the rotation rate. The angular torque profile as determined by the curvature analysis varied astoundingly little, less than by a factor of two. It corresponded to an almost linear decay of the output free energy over the angular reaction coordinate. In light of the established stepping of the load-free enzyme, and its high activation energy ($\sim$40 kJ $\cdot$ mol^{-1}), it implied an elastic power transmission between the inner rotary drive and the **c**-ring. We simulated such a device and characterized its elastic parameters.

MATERIALS AND METHODS

Chemicals

Streptactin, streptactin-sepharose, and desthiobiotin were purchased from IBA (Göttingen, Germany). Nickel-nitrilotriacetic acid horseradish peroxidase and nickel-nitrilotriacetic acid superflow were from Qiagen (Hilden, Germany). Biotin-$PEAC_5$-maleimide was from Dojindo/Gerbu (Frankfurt, Germany). Phalloidin-tetramethylrhodamine B isothiocyanate conjugate was from Fluka (Buchs, Switzerland). All other reagents were of the highest grade commercially available.

Proteins

ATP synthase

The experiments were performed with a completely Cys-less EF_0EF_1 mutant (Kuo et al., 1998) carrying a his-tag sequence at the N-terminus of each subunit β (RGSHHHHHHGM(–ATGKI . . . –β)) and a strep-tag affinity peptide at the C-terminal of subunit **c** ((C– . . . MFAVA)-SWSHPQFEK), pSE1 (Pänke et al., 2000). *E. coli* strain DK8 (Klionsky et al., 1984) was transformed with the appurtenant plasmid pSE1. Cells were collected at OD_{600} = 0.8. Membranes were purified essentially according to Wise (1990). The procedure included two additional washing steps with 5 mM Tris/HCl (pH 8), 10 mM $MgCl_2$, 0.2 mM EGTA, 10% (v/v) glycerol followed by centrifugation at 220,000 $\times$ *g* for 90 min. Membrane pellets were stored (20 mg protein/ml in 5 mM Tris/HCl (pH 8), 10 mM $MgCl_2$, 70 mM KCl, 20% (v/v) glycerol) at −80°C. Aliquots (100 mg protein) were suspended at 5 mg/ml protein in 50 mM Tris/HCl (pH 7.5), 5 mM $MgCl_2$, 1 mM K-ADP, 15% glycerol (buffer A), 1 tablet of Boehringer complete inhibitor tablets/50 ml extraction volume. *N*-octyl-β-D-glucopyranoside (25% (w/v) in H_2O) was added dropwise to an initial concentration of 1%. After stirring for 15 min on ice, additional detergent was added to a final concentration of 2.2% (w/v). Membrane protein was extracted by stirring on ice for 30 min followed by centrifugation at 100,000 $\times$ g for 90 min. Avidin was added (1 μg/ml) followed by dilution of the supernatant

to 1% (w/v) *N*-octyl-β-D-glucopyranoside with buffer B (20 mM TES (pH 7.5), 5 mM $MgCl_2$, 1 mM K-ADP, 15% (v/v) glycerol). This solution was applied batchwise to 5 ml streptactin-sepharose (settled volume, 5 mg streptactin/ml). The gel was packed into an empty NAP-10 column (Pharmacia, Freiburg, Germany), washed with 5 ml buffer B containing 1% (w/v) *N*-octyl-β-D-glucopyranoside at 0.5 ml/min. EF_OEF_1 was then eluted with 10 ml of the same buffer containing 2.5 mM desthiobiotin. Protein containing fractions were combined and batchwise adsorbed onto 1 ml nickel-NTA superflow. The gel was packed into an empty NAP-5 column (Pharmacia), washed with 1 ml 50 mM Tris/HCl (pH 7.5), 5 mM $MgCl_2$, 1% (w/v) *N*-octyl-β-D-glucopyranoside, 20 mM imidazole, 10% (v/v) glycerol and eluted with the same buffer containing 150 mM imidazole, resulting in 150 μg/ml protein. The preparation contained all eight subunits (α, β, γ, ε, **a**, **b**, and **c**) as checked by SDS electrophoresis with the Pharmacia Phast system (8-25% gradient gels) as previously described (Pänke et al., 2000). Protein determination was carried out according to Sedmak and Grossberg (1994). ATPase activity was measured with 0.1 μg protein, 50 mM Tris/HCl (pH 8.0), 3 mM $MgCl_2$, 10 mM Na-ATP, 1% *N*-octyl-β-D-glucopyranoside. Typical activities under these conditions were 70 U/mg at 37°C. The EF_1 subcomplex lacking the EF_O subunits were prepared according to Noji et al. (1999). ATPase activity was measured as above but without detergent. Typical activities under these conditions were 130 U/mg at 37°C.

Actin filaments

G-actin was prepared from acetone powder obtained from rabbit skeletal muscle as described by Pardee and Spudich (1982). The protein was briefly sonified and gel-filtrated against 2 mM Mops/KOH (pH 7.0), 0.2 mM $CaCl_2$, 2 mM ATP (buffer G). Biotinylation was carried out with a sixfold molar excess of biotin-$PEAC_5$-maleimide for 2 h at ambient temperature. Excess reagent was removed by an overnight dialysis (buffer G) followed by two successive gelfiltrations (Pharmacia PD 10/buffer G). This preparation was stored frozen in aliquots at −80°C. Before use the thawed G-actin (30 μM) was converted into fluorescently labeled F-actin by addition of 20 mM Mops/KOH (pH 7.0), 100 mM KCl, 10 mM $MgCl_2$, 30 μM phalloidin-tetramethylrhodamine B isothiocyanate conjugate (3 h/4°C) (Noji et al., 1997). Special care was taken in pipetting the labeled F-actin. The filament length varied between 0.5 and 10 μm depending on the applied shear force.

Rotation assay

Samples were placed into flow cells consisting of two coverslips (bottom, 26 × 76 mm^2; top, 21 × 26 mm^2, thickness 0.15 mm, Menzel-Gläser/Prolabor, Georgsmarienhütte, Germany) separated by parafilm strips. Protein solutions were infused in the following order (2 × 25 μl per step, 4 min incubation): 1) 0.8 μM nickel-NTA-horseradish peroxidase (Ni-NTA-HRP) conjugate in 20 mM Mops/KOH (pH 7.0), 50 mM KCl, 5 mM $MgCl_2$ (buffer R); 2) 10 mg/ml bovine serum albumin in buffer R; 3) 5 nM EF_OEF_1 in 50 mM Tris/HCl (pH 7.5), 50 mM KCl, 5 mM $MgCl_2$, 10% (v/v) glycerol, 1% (w/v) *N*-octyl-β-D-glucopyranoside (buffer S); 4) wash with buffer S; 5) 0.5 μM streptactin in buffer S; 6) wash with buffer S; 7) 200 nM biotinylated, fluorescently labeled F-actin in buffer S (7 min incubation); 8) wash with buffer S; 9) 20 mM glucose, 0.2 mg/ml glucose oxidase, 50 μg/ml catalase, 0.5% 2-mercaptoethanol, 5 mM ATP in buffer S. Deliberate omission of either one single component of the chain Ni-NTA-HRP–strep-tagged EF_OEF_1–streptactin–biotin-F-actin prevented the binding of fluorescent F-actin, as evident from the absence of fluorescent filaments within the flow cell. These results ensure that the actin filaments were attached in the correct manner. The inhibition of the ATP-driven filament rotation by *N*,*N*9-dicyclohexylcarbodiimide (DCCD), which is known to bind to the essential Asp-61 of subunit **c** and thereby interfere with the protonation of this residue, was not observed. The interaction between the **a** subunit and the **c**-ring is probably weakened by the detergent. The loss of protonic coupling does not affect the implications of this work. The goal was to test whether there is an elastic power transmission between immobilized F_1 and the **c**-ring of F_O. The elasticity in the stator portion, involving subunits **a** and **b**, is another topic (see Fig. 1). The ADP content of the ATP stock solution was measured photometrically after chromatophoric separation and came to 1% of the ATP amount. Under these conditions (5 mM ATP, 50 μM ADP and phosphate, 5 mM Mg^{2+}, pH 7.0, 0.1 M ionic strength, 20°C) the Standard Gibbs energy was 28.6 kJ/mol^{-1}, resulting in a Gibbs energy of 64.0 kJ/mol^{-1} (Krab and Vanwezel, 1992; Pänke and Rumberg, 1997).

Video microscopy

An inverted fluorescence microscope (IX70, Olympus (Hamburg, Germany), lens PlanApo 100×/1.40 oil, fluorescence cube MWIG) was equipped with a silicone intensified tube camera (C 2400-08, Hamamatsu, Herrsching, Germany) and connected to a VHS-PAL video recorder (25 frames per second). With this setup filaments of 5 μm length appeared as 3 cm long rods on a 14″ monitor. The flow was loaded with freshly extracted and chromatographed samples of EF_OEF_1 labeled with actin filaments and single molecule rotation was studied up to 30 min after loading. Video data were captured (frame grabber FlashBus, Integral Technologies, Indianapolis, IN) and further processed by using the software ImagePro4.0 (Media Cybernetics, Silver Spring, MD) and Matlab 5.2 (The Math Works, Natick, MA). All rotation experiments were carried out in a thermostated laboratory at 20°C.

Digital image analysis

The digitized images were analyzed by a home-made routine using the program Matlab 5.2. The analysis of rotating filaments included the following steps. 1) About 1000 sequential image frames of a given rotating filament were superimposed and averaged to yield the position of the rotation axis (the position of the rotary enzyme). The distances from the rotation axis to the filament ends were read out from 10 to 20 selected video frames (where the filament bending was minimal) and corrected for the apparent half-width of the filament (0.17–0.25 μm, depending on the fluorescence intensity). Filaments with an asymmetric position of the axis were selected for analysis. The axis was typically 0.4–0.8 μm apart from the filament end. 2) For each frame the angular orientation of the filament, θ', was at first grossly determined with a precision of ±10° by analysis of the luminosity distribution around the rotation axis. A local 2D-coordinate system with axes x' and y' was introduced. The axis x' was directed toward the long end of the filament. In the second step the angular position θ of the filament was determined more precisely by the linear least-squares analysis of a small area around the rotation axis (usually, a circle with a radius of 0.75–1.0 μm). The minimization function

$$\chi^2(a, b) = \sum_{x_j' \le 0} C_j (y_j' - a \cdot x_j')^2 + \sum_{x_j' > 0} C_j (y_j' - a \cdot x_j' + b \cdot x'^2_j)^2$$

approximated the short end of the filament by a straight line and the long end by a parabola (C_j was the luminosity of the pixel with coordinates (x', y'), $a = \tan(\theta)$, and the parameter b accounted for the curvature of the long end of the filament). Standard uncertainties of the parameters a and b were calculated by the covariance matrix of normally distributed errors used in the least-squares analysis (see, e.g., Bevington, 1969, Chapter 6). A new local system of coordinates (x, y) was then defined by the rotation of the axes by the angle θ. 3) A deformation of the filament relative to the straight line (which extrapolated the axial direction) was determined by the linear least-squares analysis of a greater area around the rotation axis (1.5–2.0 μm). The ground eigenfunction $\tilde{y}_0(x)$ (see Eq. 17 in Cherepanov and Junge, 2001) was used as a model curve for this deformation; its amplitude was the only variable fit parameter. The maximal deviation of the fitted model curve from the extrapolated straight line at the free end of the filament (in μm) was termed A_0.

Superposition of the images with the same angular position θ_m ($m = 1, 2, \ldots, 60$) of each rotating filament was done by Matlab 5.2. The average deformation curve in the superimposed images was determined by the same procedure as described above.

The analysis of nonrotating (blocked) filaments was slightly different. The images were initially superimposed and averaged. The position where the filament was fixed on the solid support corresponded to the minimum width of the apparent filament and to the maximum of the luminosity of the averaged image. The uncertainty of this position did not exceed 2 pixels (0.15 μm). The distance from the fixed position to the free end of the filament (the working length) was determined as described. The orientation of the fixed part of the filament (the angle θ) was determined by the least-squares analysis of the average imaged as in stage (2) above. The deformation of the free part of the filament relative to the straight line was determined by the linear least-squares analysis using the two lowest eigenfunctions $\tilde{y}_0(x)$ and $\tilde{y}_1(x)$, their amplitudes A_0 and A_1 were variable parameters.

RESULTS AND DISCUSSION

Control of the enzyme-powered rotation by bulk versus surface viscosity, surface friction, and obstacles

Actin filaments were attached to the **c**-ring of F_OF_1 constructs as described in Materials and Methods (see Fig. 1 for an illustration). The procedure yielded up to 5% of rotating filaments in a typical preparation (see also Pänke et al., 2000). A large fraction of nonrotating filaments had a fluctuating free end, apparently because they were attached to several enzyme molecules at once. This view was based on the following observation. When passing a stream of fluid over the filament/enzyme covered glass slide, we observed discrete sequential detachment steps for such filaments and concomitant progression of the kink toward the *free end*, which was oriented along the stream lines. The stepping exposed the discrete attachment sites.

The angular progression of rotating filaments was usually rather nonuniform, evidently due to interaction with the surface. Only a very low fraction of rotating filaments demonstrated a regular motion without breaks and extended resting periods. We analyzed the dynamics of such "well behaved" filaments.

Video frames of a rotating 3-μm-long actin filament are shown in Fig. 2, *A–C*. This sequential series of video frames (exposure time of 40 ms) was taken at intervals of 400 ms. For comparison, a blocked filament of similar length with a fluctuating free end is shown in Fig. 2 *D* (10 sequential video frames taken at intervals of 400 ms). A closer inspection revealed, however, that the motion of rotating filament was frequently impeded. Fig. 3 documents the dynamics of the same rotating filament in a higher resolution (200 ms intervals between the frames). In the first and second rows of Fig. 3 the filament rotated, driven by the hydrolysis of ATP. In the last row the rotation was obstructed, apparently because the filament had hit an obstacle on the surface of the solid support. In all frames, with and without rotation, the filament was elastically deformed by the torque generated by the enzyme. In the theoretical article (Cherepanov and Junge, 2001) we have demonstrated that the overall curvature (at equal torque) is not very different depending on whether the counter-torque is due to viscous drag on the filament or to an obstacle at its free end.

The angular progression of this particular filament was determined by the analysis of 1800 sequential video frames taken at intervals of 40 ms (see Fig. 4). In total, the rotation was rather uniform, with only short resting intervals and fluctuations. The average angular velocity $\bar{V}$ of this filament, as calculated for the whole trajectory, was 0.25 revolutions/s. We compared this rate with the calculated one based on Stokes' theory of flow around a rotating cylinder. According to this theory (see Hunt et al., 1994), the average angular rate, $\bar{V}$, is determined by the torque of enzyme, $\bar{T}$, the radius of the filament, R, its length, L, and the solvent viscosity, η:

$$\bar{V} = \frac{3\bar{T}}{4\pi\eta L^3}\,(\ln(L/2R) - 0.447) \qquad (1)$$

The working length of this filament (i.e., the distance from the rotation axis to the long end) was read out from the video frames and corrected for the width of the diffraction-limited image as described in Materials and Methods. This yielded the L value of 2.6 μm. Taking the effective radius of F-actin as 2.8 nm (Mendelson and Morris, 1997), and the viscosity of bulk water (10^{-3} N · m^{-2} · s) we arrived at an average torque of only 20 pN · nm. Another way to estimate

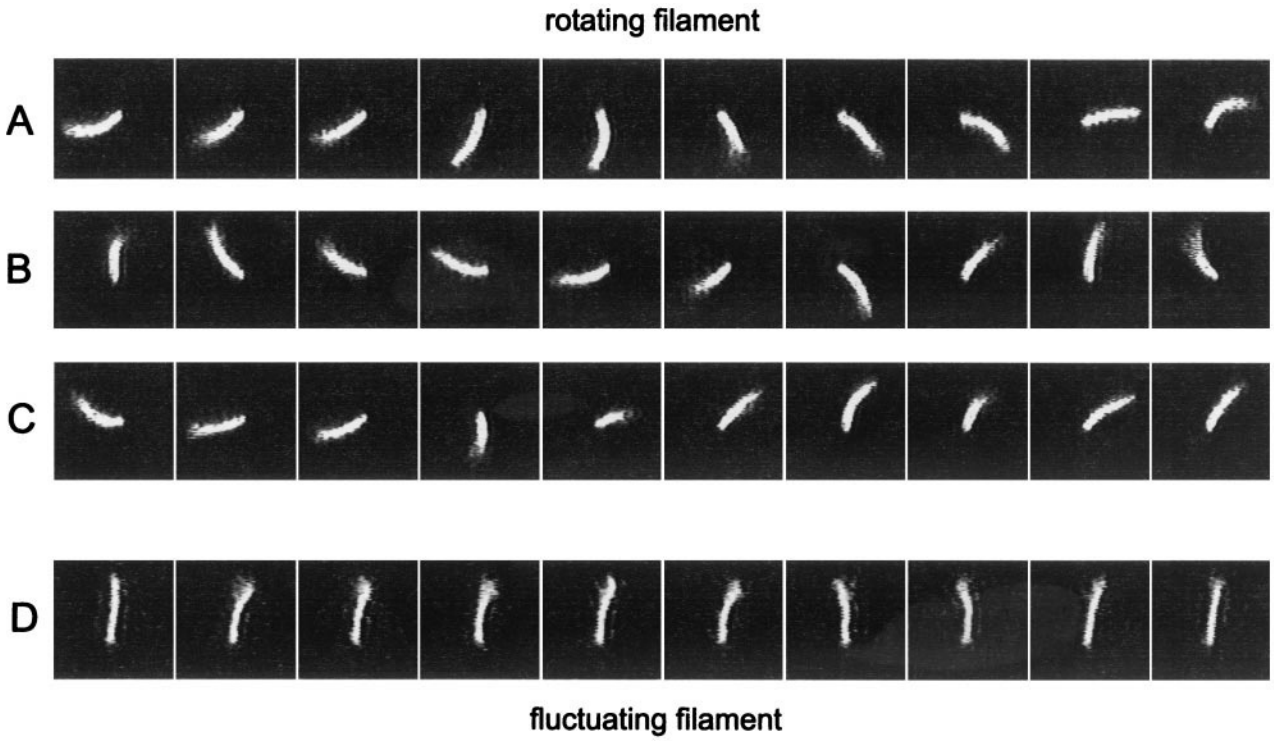

FIGURE 2 Video records of a rotating (*A–C*) and a blocked fluorescent actin filament (*D*). The filaments were attached to the **c**-ring of F_OF_1 constructs as illustrated in Fig. 1. The video frames were taken sequentially at intervals of 400 ms.

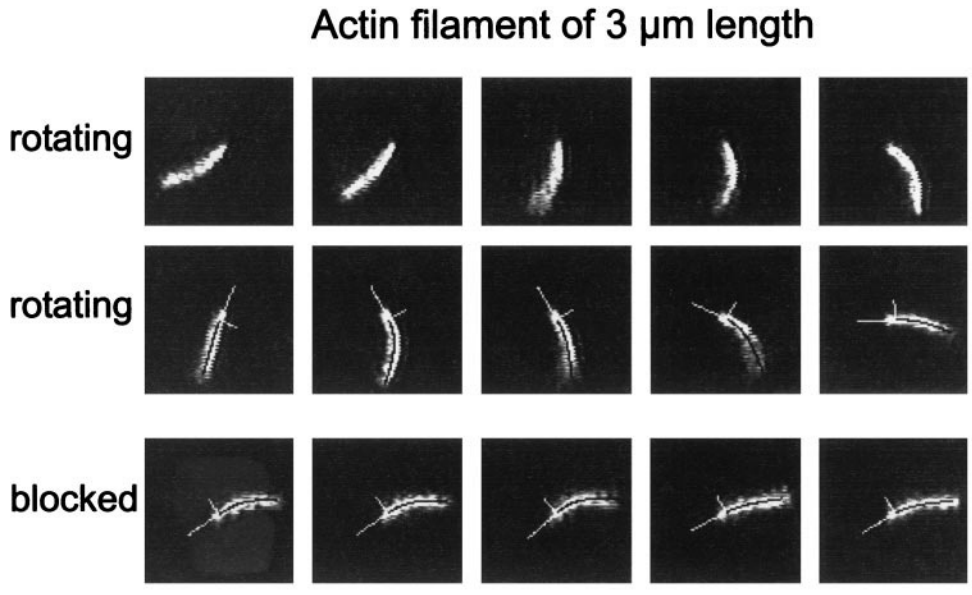

FIGURE 3 Video frames of the rotating actin filament from Fig. 2 taken sequentially at intervals of 200 ms. The first and second rows represent rotary motion driven by the hydrolysis of ATP, the third row blockage by an obstacle on the surface. Whether rotating or nonrotating, the filament was elastically deformed by enzyme-generated torque. For each video frame the angular position of the filament at the rotation axis was determined by a least-square fitting procedure as described in Materials and Methods. In the last two rows the extrapolated angular positions at the rotation axis are shown as white lines. The deflection of the curved filament from the extrapolated line is shown in black. It was calculated and fitted as given under Materials and Methods.

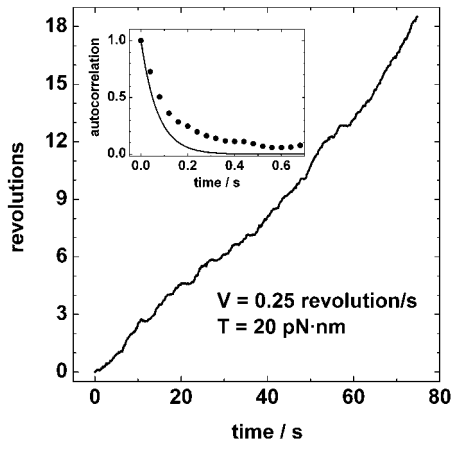

FIGURE 4 Trajectory of the rotational progression of the same filament as shown in Fig. 3. The average angular velocity calculated for the shown segment of the trajectory (1800 video frames) was 0.25 revolution/s; the respective torque as calculated by Eq. 1 was only 20 pN · nm. The *inset* shows the autocorrelation function of the progression (*circles*). Its deviation from the theoretical prediction based on the Stokes' flow theory (*solid line*) was indicative of surface contacts.

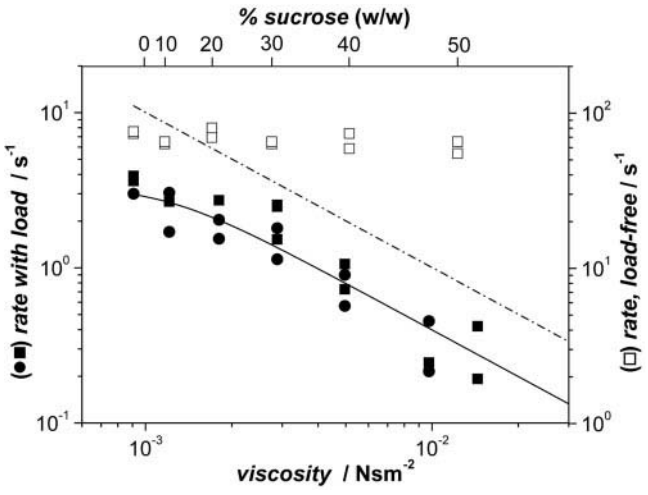

FIGURE 5 The average rotation rate of actin filaments expressed in revolutions per second as a function of the bulk viscosity at 20°C. The viscosity was varied by the addition of sucrose (concentration given in the top scale); the related viscosity values are taken from Fasman (1975). Open squares show the rate of ATP hydrolysis of solubilized, filament, and thus load-free F_1 that was obtained by standard biochemical activity assay. It served as a control for the enzyme activity per se. Filled symbols denote the rates of filament rotation driven by F_OF_1 (*circles*) and by F_1 (*squares*), respectively. The filament length was 1.0 ± 0.1 μm in both cases. In the case of F_1 the actin filament was connected to subunit γ as in Noji et al. (1999); in the case of F_OF_1 to the **c**-ring as in Pänke et al. (2000). The linear portions of the inserted curves were calculated according to Eq. 1, where the rotational rate equals the angular rate, $\bar{V}$, divided by 2π. η is the bulk viscosity given by the sucrose concentration; L is 1 μm, the length of the filament; R is 2.8 nm, the radius of the actin filament. The average torque was taken as $\bar{T}$ = 20 pN · nm (*solid line*) and 51 pN · nm (*dashed line*), respectively.

the torque was to assume perfect coupling (no slip) and to consider the molar free energy difference of ATP hydrolysis, ΔG = 64 kJ/mol (see Materials and Methods). The free energy difference is related to the average torque, $\bar{T}$, by the rotation angle per ATP, $2\pi\bar{T}/3 = \Delta G/N_A$, with N_A denoting Avogadro's number.

Based thereupon, we calculated the average torque under ideal conditions (no slip, operation very close to thermodynamic equilibrium) as 51 pN · nm, 2.5 times greater than based on the assumption that the filament felt the viscous drag of bulk water. This assumption was made in all previous estimates of the average torque (e.g., Yasuda et al., 1998; Sambongi et al., 1999). A probable reason for the discrepancy was a greater apparent viscosity because the filament moved closely, i.e., at nanometer distance, over the protein-covered solid support. It is known that the compression of flow lines between a moving rod and a surface increases the viscosity considerably if the rod moves close to the surface (Happel and Brenner, 1983). Direct contact between the filament and the surface might have added to this effect (surface friction and obstacles).

If the rotation of the filament was controlled by viscous drag of a homogeneous liquid, a high positive cross-correlation between the momentary angular velocity and the filament curvature was expected: a greater curvature corresponding to greater velocity because of greater torque. Such distinctly positive correlation, however, was not observed (data not documented). Instead, the correlation was irregular with positive, zero, and even negative figures, hardly consistent with friction in a homogeneous medium. The same inconsistency followed from the curvature-curvature autocorrelation function, which is shown in the inset of Fig. 4. The expected behavior (see Eq. 41 in the companion paper (Cherepanov and Junge, 2001)) is represented by a solid line and the experimentally observed behavior by points. Broadly speaking, the expected autocorrelation curve reflects the viscoelastic relaxation of the actin filament's ground mode. In contrast to the former, the observed dependence showed a long tail, which we attributed to surface contacts.

Was there any role of the bulk viscosity at all? We addressed this question by measuring the rate of rotation of actin filaments when the bulk viscosity was increased by the addition of sucrose. The result is depicted in Fig. 5. Filled symbols show the rotation rate of F_OF_1 filament constructs as a function of the bulk viscosity (lower scale). The top scale gives percent sucrose. Open squares show the rate of ATP hydrolysis of the filament-free, solubilized F_1 as a control for the enzyme activity per se. It was independent of the sucrose concentration. Straight lines represent the expected reciprocal behavior between the rate of rotation and the bulk solvent viscosity according to Eq. 1. It was obvious that the viscosity determined the rotation rate perfectly well at higher sucrose concentration. At low viscosity surface friction was apparent, as also suggested by the correlation

analysis above. The solid line at high viscosity was calculated under the assumption that the average torque was 20 pN · nm and the broken line for 51 pN · nm. In both cases it was assumed that the filament "felt" the viscosity of the bulk, so that Eq. 1 was valid. That the data points (see also solid line) were lower than expected for a perfectly coupled enzyme (*broken line*) hinted at ~2.5 times greater effective viscosity at the surface than in the bulk, at least for our data. This has limited the precision of previous attempts to calculate the torque from the rotation rate and the bulk viscosity.

The enzyme torque obtained by the curvature and the flexural rigidity of actin filaments

We attempted to more precisely gauge the torque of the rotary enzyme by the curvature of enzyme-linked actin filaments as outlined in the theoretical article (Cherepanov and Junge, 2001). The elastic rigidity of F-actin filaments, as documented by various groups of authors, was found to be highly dependent on the experimental conditions (in particular, on the amount of bound phalloidin) and varied by one order of magnitude (see, e.g., Yanagida et al., 1984; Isambert et al., 1995; Xu et al., 1998). Moreover, the flexural rigidity of different filaments in similar preparations varied between $3.0 \pm 0.5 \cdot 10^{-26}$ N · m^2 and $1.6 \pm 0.5 \cdot 10^{-25}$ N · m^2 (Gittes et al., 1993). We analyzed the thermal dynamics of 13 fluctuating and nonrotating filaments as described in Material and Methods (see also Fig. 2 *D* and the previous section) and found a flexural rigidity of $8.2 \pm 3.0 \cdot 10^{-26}$ N · m^2 (ranging between $3.9 \cdot 10^{-26}$ N · m^2 and $12.6 \cdot 10^{-26}$ N · m^2). To overcome the ambiguity because of large spread between filaments, we determined the flexural rigidity of any rotating filament by the analysis of its own thermal fluctuations in the course of rotation, as described below, and we compared this value with the elastic properties of blocked filaments of the same preparation and of the same batch on the same coverslide that contained the rotating filaments.

Video records of several rotating filaments (at a working length of 2–4 μm) were analyzed for the momentary curvature and angular dynamics. The angular positions of filaments at the rotation axis were determined for each video frame by the least-squares analysis as described in Materials and Methods. The standard uncertainty of the estimated angular position, σ_θ, was calculated for each video frame by the covariance matrix of normally distributed errors (Bevington, 1969). For different rotating filaments average values of σ_θ ranged between 2.6 and 5.0° (the accuracy depended mainly on the length of the short part of the filaments). The extrapolated axes and the calculated deformation curves are documented in the last two rows of Fig. 3 by white and black lines, respectively. The free end displacements perpendicular to the extrapolated directions, A_0, were then read out. The filament curvature at the rotation axis was directly related to the displacement A_0 by the equation $y''(x)|_{x=0} = (\delta_0/L)^2 A_0$ (see Cherepanov and Junge, 2001). The average standard error of the curvature estimation, $L^{-1}\sigma_A$, varied between 0.11 and 0.16 for different filaments and was only weakly dependent on the working length (see the discussion of the possible errors below). The distribution of the displacements, $\rho(A_0)$, calculated for the whole trajectory from Fig. 4 was plotted in Fig. 6 by filled circles. For comparison, the distributions of amplitudes of the two lowest eigenfunctions, $\rho_0(A_0)$ and $\rho_1(A_1)$, calculated for a blocked filament from the same batch (see the last row of Fig. 2), are documented in Fig. 6 by open triangles and open squares, respectively (for the sake of clarity, the amplitude A_1 in this figure was scaled by the factor $(\delta_1/\delta_0)^2$, see Eq. 34 in Cherepanov and Junge, 2001).

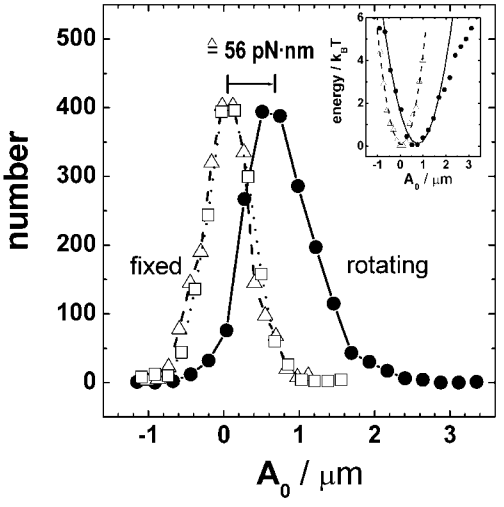

FIGURE 6 Histograms of the maximal displacements of two filaments from the extrapolated directions, A_0. They were calculated for rotating (*circles* and *solid line*, the trajectory from Fig. 4) and nonrotating (*triangles* and *broken line*, the trajectory was not documented) filaments with slightly different lengths, 2.0 and 2.6 μm. The different width of the profiles was caused by the different langth. The distribution of the scaled amplitude of the second eigenmode, $(\delta_1/\delta_0)^2 A_1$, calculated for the nonrotating filament, is shown by open squares and dotted line. The shift of the peak position of rotating filament corresponded to the torque value of 56 pN · nm. The *inset* shows logarithmic replots of the data points and a parabolic approximation representing the potential profiles of elastically deformable actin cantilevers.

The peak position and the distribution width differed between the rotating and nonrotating filaments of slightly different working length. The shift of the peak position was straightforwardly related to the enzyme-generated torque. The narrower widths of the $\rho_0(A_0)$ and $\rho_1(A_1)$ distributions were attributable to the smaller working length of the nonrotating filament, namely 2.0 μm vs. 2.6 μm for the rotating filament (an almost perfect agreement was after the length correction). It follows from the analysis of thermal fluctuations of an actin cantilever that the negative logarithm of $\rho_0(A_0)$ and $\rho_1(A_1)$ (nonrotating cantilever) and of $\rho(A_0)$

TABLE 1 The viscoelastic characteristics of six uniformly rotating F_OF_1–F-actin complexes

Filament No.	Working length L (μm)	Number of Frames	Average Angular Rate $\bar{V}$ (revolution/s)	Torque by Velocity $\bar{T}_{vel}$, (pN · nm)	Flexural Rigidity EI, $\times 10^{26}$ N · m^2	Torque by Curvature $\bar{T}_{curv}$ (pN · nm)
1	1.4	739	0.42	6	6.0 ± 0.3	50 ± 7
2	1.8	541	1.04	30	8.9 ± 0.8	41 ± 8
3	1.9	350	0.41	14	4.8 ± 0.9	47 ± 4
4	2.1	2536	0.50	19	9.4 ± 0.6	49 ± 4
5	2.6	1871	0.25	20	11 ± 0.5	56 ± 4
6	2.6	3044	0.10	8	10 ± 0.7	58 ± 5
Mean				16 ± 9	8.4 ± 1.0	50 ± 6

(rotating cantilever) characterizes the energy profile of elastic deformations. Logarithmic replots of $\rho_0(A_0)$ and $\rho(A_0)$ are shown in the inset to Fig. 6. They approximated the expected parabolic potential curve of an elastically deformed cantilever fairly well. The flexural rigidity of both filaments, EI, was calculated from the width of the respective distributions according to Eqs. 34 and 38 in Cherepanov and Junge, 2001. The values of EI obtained from the three data fits, $1.06 \pm 0.04 \cdot 10^{-25}$, $1.21 \pm 0.03 \cdot 10^{-25}$ (nonrotating filament), and $1.16 \pm 0.05 \cdot 10^{-25}$ N · m^2 (rotating filament) were consistent and corresponded to elastic moduli of $2.2 \cdot 10^9$, $2.5 \cdot 10^9$, and $2.4 \cdot 10^9$ N · m^{-2}, respectively, when assuming an average cylindrical radius for F-actin of 2.8 nm (Mendelson and Morris, 1997). The figures for flexural rigidity in these batches of F-actin were somewhat greater than the average values of $6-8 \cdot 10^{-26}$ N · m^2 that were previously reported by the analysis of bending fluctuations of unconstrained diffusing filaments (Gittes et al., 1993; Isambert et al., 1995), of twisting fluctuations of a immobilized and stretched F-actin filaments (Tsuda et al., 1996; Yasuda et al., 1996; and this work (see above)).

By using the above figures for the flexural rigidity, $EI = 1.1 \cdot 10^{-25}\ N \cdot m^2$, and for the average deflection $\bar{A}_0$ of the rotating filament, we calculated by Eq. 37 in Cherepanov and Junge, 2001 the average torque of the enzyme, $\bar{T}$. The result, $\bar{T} = 56$ pN · nm, agreed reasonably well with the free energy of ATP hydrolysis (at least 51 pN · nm) under the given experimental conditions (see Materials and Methods). The results of the analogous analysis of six uniformly rotating filaments are presented in Table 1. The curvature analysis yielded the average torque of 50 ± 6 pN · nm, whereas the method based on the Stokes' theory gave only a value of 16 ± 9 pN · nm. The agreement of the former with the one expected for fully coupled ATP hydrolysis proved the absence of any slip between ATP hydrolysis in F_1 and the rotation of the **c**-ring of F_O.

The curvature analysis of both rotating and nonrotating filaments included several types of noise due to the limited resolution of video images, Brownian fluctuations, motion out of the focal plane, etc. It was worthwhile to estimate the probable uncertainty of the results; in particular, how the accuracy of the averaging depended on the number of analyzed video frames.

Due to the limited resolution of video system (which depended on the fluorescence intensity), the standard uncertainties of the estimated angular position (σ_θ) and the relative deflection ($L^{-1}\sigma_A$) were determined by the apparent width of the filament (0.35–0.5 μm), the length of its short part (0.4–0.8 μm), and the working length (1.4–2.6 μm). The average uncertainty of both these parameters, $\sigma_\theta + L^{-1}\sigma_A$, calculated separately for six filaments, ranged between 0.15 and 0.24. Because we did not expect a systematic bias in these estimates, the error of this kind had to decrease as $N^{-1/2}$ for N analyzed video frames and, therefore, did not essentially affect the results. The same conclusion followed from the consistent values of flexural rigidity obtained by the analysis of two independent eigenmodes of blocked filaments. The standard errors for the estimated flexural rigidity in Table 1 were calculated by the covariance matrix used in the least-squares minimization.

Other kinds of error might arise due to random or systematic mistakes in the estimation of the filament length (light diffraction and uncertainty in the position where the blocked filaments were fixed). Such error introduced a systematic bias into the analysis of a given series of video frames and could not be eliminated by averaging. In this aspect, however, the curvature analysis was more precise than the common approach based on the average rate of rotation: the latter method has the third-power dependence on the filament length (see Eq. 1), whereas the flexural rigidity, calculated by the width of curvature distribution according to Eqs. 34 and 38 in Cherepanov and Junge, 2001, is proportional to the first power of length (the shift of the peak position is even less dependent on the filament length). Thus, a likely error of ±0.3 μm (the diffraction limit) in the length of a 2-μm-long filament would lead to a 50% error in the torque estimation by the velocity and only to a 15% error by the curvature.

Brownian motion of filaments out of the focal plan (along the z axis) was another source of noise. It was not essential for short filaments, because their apparent length was almost not affected by these fluctuations. A somewhat greater apparent torque found for the two longest (2.6 μm) filaments might, however, be caused by slightly increased apparent curvature due to fluctuations in the z dimension. To minimize such effects we calculated the curvature in a

small area (typically a sphere with radius of 1.5 μm, see Materials and Methods) around the rotation axis.

Because the enzyme-induced curvature of a given filament was blurred by Brownian fluctuations, the averaging of their effects was critical for the accuracy of the results. As known from standard textbooks of mathematical statistics, the mean of n independent measurements, $\bar{x} = 1/n \sum_{v=1}^{n} x_v$, obeys Student's distribution,

$$p_{n-1}(t) = (\pi(n-1))^{-1/2} \cdot \Gamma\left(\frac{n}{2}\right) \Big/ \Gamma\left(\frac{n-1}{2}\right) \cdot (1 + t^2/(n-1))^{-n/2},$$

where the variables x_v have the theoretical mean value x_0 and the dispersion σ, and the parameter t represents a normalized deviation of the experimental mean from the theoretical one, $t = \sqrt{n-1}(\bar{x} - x_0)/\sigma$. The width of the non-normalized Student's distribution, $2\sigma/\sqrt{n-1}$, gives the standard error of n independent measurements. For example, the calculated distribution $\rho(A_0)$ in Fig. 6 was based on ~360 independent frames (the observed correlation time of this filament was ~200 ms, see inset to Fig. 4, so neighboring video frames taken at intervals of 40 ms were not independent). This gave the standard error for the torque estimation of ± 8 pN · nm, reasonably close to the observed error of ± 6 pN · nm resulting from the analysis of six rotating filaments (see Table 1). We concluded that the uncertainty of the curvature analysis was determined mainly by Brownian impacts. The standard errors calculated by Student's distribution are summarized in Table 1.

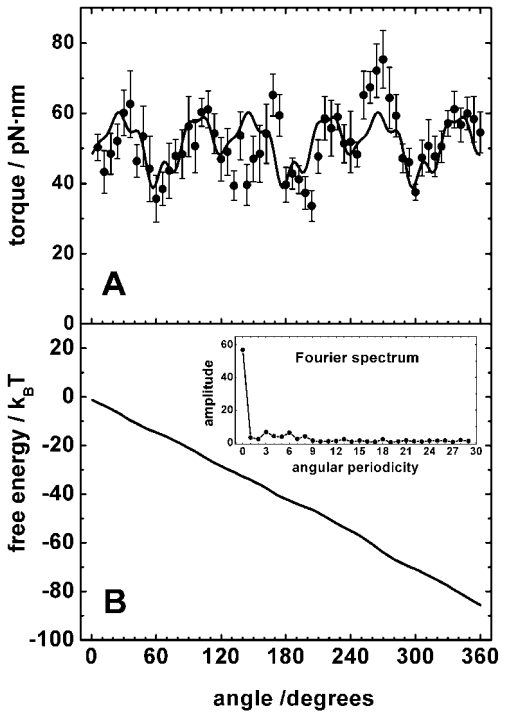

FIGURE 7 The angular dependence of the average output torque (*A*) and the respective free energy profile (*B*) of the F_OF_1 construct. This profile was calculated from very many turnovers of six rotating filaments. The original data of one filament are shown in Figs. 3 and 4. The inset to the bottom panel shows the Fourier spectrum of the experimental points from the top panel (*circles*). The smooth curve on the top panel was obtained as a filtered back-transform of the Fourier spectrum (for details, see text). It represents an idealized angular dependence of the torque under the assumption of a threefold symmetry of the torque generator. (Thereby the smooth curve differs from an unbiased fit to the data!)

The angular dependence of the average torque of ATP synthase

During turnover, each angular position of the rotating enzymes was occupied many times. We determined the average angular dependence of the torque as generated by six different F_1F_O molecules represented in Table 1 during very many rounds of rotation by analyzing the elastic deformation of the attached actin filaments. The image frames for each filament were sorted by the extrapolated angular position of the filament at the axis of rotation (see Fig. 4). Each revolution (360°) was divided into 60 sectors (BINS), six degrees wide. Images falling into one particular BIN, typically 30, were superimposed and their average deflection curves were calculated (see Materials and Methods). The angular dependence of the average torque at the **c**-ring was determined for the six F_1F_O constructs. The results were phase-matched and then averaged point by point. (The relative phase shifts of the angular profiles were determined by the RMSD optimization.) The mean torque and the standard error were calculated separately for each angular position. These parameters are shown in Fig. 7 *A* by circles and bars, respectively. A weak C_3-symmetrical progression is apparent by inspection. The blurring of the profile was not caused by errors in the phase-matching procedure. It was evident in the analysis of every single filament. The Fourier spectrum of the experimental data from Fig. 7 A is plotted as the inset to Fig. 7 *B*. Whereas the major spectral component was independent of the angle (constant torque), two much smaller Fourier components revealed C_3 and C_6 symmetries, respectively. The smooth curve $\bar{\boldsymbol{T}}(\theta)$ in Fig. 7 *A* represents the back-transform of the Fourier spectrum (Fig. 7 *B*, *inset*) after filtering to include only the nine lowest harmonics matching the threefold symmetry C_{3n} ($n = 0, 1, \ldots, 8$). The resulting interpolated curve, $\bar{\boldsymbol{T}}(\theta)$, represents an idealized, noise-filtered angular dependence of the output torque of F_1F_O.

A remarkable feature of the analyzed filaments listed in Table 1 was a rather weak variation of the torque as function of the rotary position. The maximum and the minimum of the averaged torque differed typically only by a factor of two. Accordingly, the integrated torque over the angle, the output free energy profile, $\Delta G(\theta)$, yielded a rather smooth, almost linearly decreasing function (see Fig. 7 *B*). Activa-

tion barriers were absent. The difference covered over an angular domain of 120° was ~30 k_BT, which was equivalent to the free energy of hydrolysis of one molecule ATP at the given experimental conditions, namely 64 kJ/mol. In light of the known three (six-) stepped angular progression of isolated, load-free F_1 we asked for the origin of this smooth decay.

Elastic coupling between F_1 and F_O

If the two portions of the enzyme are separated from each other and running freely, i.e., without external load, their turnover rate is characterized by rather high Arrhenius activation energies ranging between 40 and 60 kJ/mol (for F_1, hydrolyzing ATP, see Al-Shawi et al., 1997, and for exposed F_O, conducting protons, see Althoff et al., 1990). The consequence of such barriers, a three (six)-fold stepping of F_1 has been experimentally established (see Introduction).

Because F_1 and F_O possess different axial symmetry (C_3 and C_{10}–C_{14}, respectively), elastic deformations have been considered as important for catalytic operation of ATP synthase (Junge et al., 1997; Wang and Oster, 1998; Syroeshkin et al., 1998; Cherepanov et al., 1999; Junge, 1999; Pänke and Rumberg, 1999; Leslie and Walker, 2000). Elastic deformations might occur both in the central shaft consisting of subunits γ and ε and in the long parallelogram of subunits **b** in the stator between F_1 and F_O. The C-terminal helical domain of subunit β carrying the highly conserved DELSEED motif might be able to pick up elastic energy when acting as a lever, which lifts up to or swings down from the nearly immobile N-terminal domain of β during catalysis. If the angular progression in F_1 was rigidly connected with the motion of the **c**-ring in F_O, the activation barrier could rise up to the sum of the activation energies of the two components of the enzyme (≈100 kJ/mol), a kinetically highly unfavorable situation. A flexible power transmission, however, was expected to smooth the free energy profile and to increase the kinetic efficiency of the coupled enzyme.

We scrutinized how elastic coupling, taking alone the torsional deformation of the γ subunit, might smooth the output torque at the **c**-ring, thereby positively affecting the turnover rate of the enzyme. As a very crude model we treated the γ subunit as an elastic rod with radius $r_\gamma \approx$ 0.8 nm and effective length $L_\gamma \approx 6$ nm (see Fig. 1 for an illustration). If twisted by the torsional angle θ_γ, it accumulates the elastic energy F_γ (see Cherepanov et al., 1999):

$$F_\gamma(\theta) = \frac{\pi R_\gamma^4 E_\gamma}{8L_\gamma(1+\sigma)}\theta_\gamma^2 \qquad (2)$$

Here E_γ denotes the longitudinal Young modulus of γ, and σ the Poisson ratio (~0.5 for most elastic materials).

Let the variables θ_1 and θ_2 denote the internal (F_1 motor) and external (filament at the axis) angular coordinates, respectively. $\boldsymbol{T}_A(\theta_1)$ is the angular input torque of the driving motor, and $V(\theta_1)$ the respective potential energy: $\boldsymbol{T}_A(\theta_1) = -(\partial V/\partial\theta_1)$. The output torque as a function of the external coordinate, $\boldsymbol{T}_B(\theta_2)$, will differ from the input torque depending on the elastic energy stored in γ as described by Eq. 2. In the case considered, where the intrinsic dynamical relaxation of F_1 is fast compared to the slow relaxation of the long actin filament, the driving motor operates very close to thermal equilibrium, almost at stall. Thereby, the output torque results from a quasi-equilibrium average over the different motor states: the average torque is denoted $\overline{\boldsymbol{T}_B}(\theta_2)$. Both $\boldsymbol{T}_A(\theta_1)$ and $\overline{\boldsymbol{T}_B}(\theta_2)$ are periodic functions with the major period $2\pi/3$. The full potential energy of the system is the sum of $V(\theta_1)$ and $F_\gamma(\theta_1 - \theta_2)$:

$$U(\theta_1, \theta_2) = V(\theta_1) + g\cdot(\theta_1 - \theta_2)^2 \qquad (3)$$

where $g = \pi R_\gamma^4 E_\gamma / 8 L_\gamma (1+\sigma)$; see Eq. 2. The average potential energy, $\bar{U}(\theta_2)$, and the average output torque, $\overline{\boldsymbol{T}_B}(\theta_2)$, can be found by evaluating Boltzmann's distribution:

$$\bar{U}(\theta_2) = \frac{\int_{-\infty}^{\infty} U(\theta_1,\theta_2)\cdot\exp(-U(\theta_1,\theta_2)/k_BT)\,d\theta_1}{\int_{-\infty}^{\infty}\exp(-U(\theta_1,\theta_2)/k_BT)\,d\theta_1} \qquad (4)$$

$$\overline{\boldsymbol{T}_B}(\theta_2) = \frac{\int_{-\infty}^{\infty} 2g\cdot(\theta_1-\theta_2)\cdot\exp(-U(\theta_1,\theta_2)/k_BT)\,d\theta_1}{\int_{-\infty}^{\infty}\exp(-U(\theta_1,\theta_2)/k_BT)\,d\theta_1} \qquad (5)$$

We modeled the behavior assuming that the input energy profile of the driving motor, F_1, was simply the sum of linear and sinusoidal terms: $V(\theta_1) = -\boldsymbol{T}_1\cdot\theta_1 + \boldsymbol{T}_2\sin(\theta_1)$. Fig. 8 (*top*) shows how the expected output energy profile $\bar{U}(\theta_2)$ depends on the elasticity of the transmission. The parameter T_1 was chosen equal to 50 pN · nm, corresponding to the free energy of ATP hydrolysis of 62 kJ/mol; the parameter T_2 was chosen as 160 pN · nm, so that the activation barrier on the reaction coordinate θ_1 had the height of 40 kJ/mol (*solid line* in Fig. 8, *top*). The output energy profiles $\bar{U}(\theta_2)$ were calculated for different elasticities of the transmission by numerical integration of Eq. 4. They are shown in Fig. 8, *top* by various types of broken lines. It is obvious that the

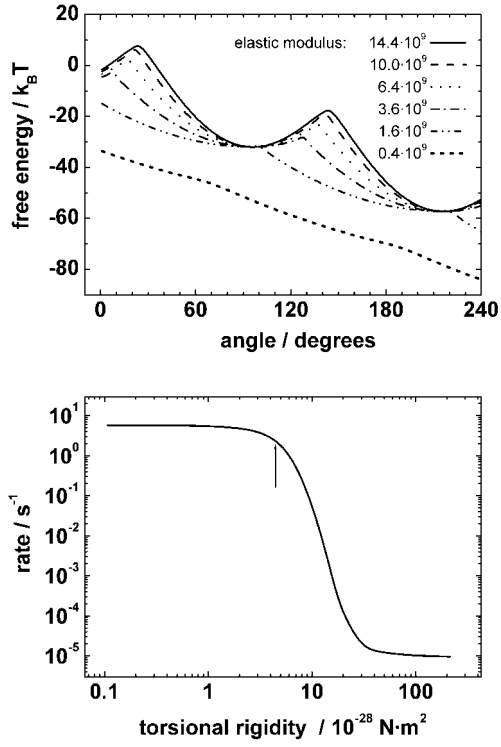

FIGURE 8 Simulation of the angular free energy profile of a C_3-symmetrical rotary engine with elastic power transmission under variation of the elastic modulus. *Top panel*: The angular dependence of the output free energy strictly reproduces the internal one in the case of an inflexible transmission (*solid line*). A soft transmission, however, smoothes the output dependence (broken lines were calculated for decreasing elastic modulus in $N \cdot m^{-2}$ as indicated). The curves were calculated by Eq. 4 starting from a modulated sinusoidal internal profile as described in the text. *Bottom panel*: The rotation rate of this motor when loaded by an actin filament moving in viscous medium. The dependence was calculated by Eq. 6 describing diffusion in a periodic potential. The arrow indicates the assumed torsional rigidity of the γ subunit serving as a rough estimate for the elasticity of F_1F_O transmission.

more flexible the transmission, the smoother the output energy profile.

To avoid misunderstanding Fig. 8, *top*, it is worth mentioning that the difference between two energies on any curve is always the same, namely 62 kJ/mol $\cong$ 25 k_BT, when taken at two angular positions that are spaced by 120° apart (as originally assumed). The absolute height of the profiles, however, is arbitrary, as always for potential energies.

The free energy profiles along the angular reaction coordinate depicted in Fig. 8, *top*, lead to the obvious conclusion that the enzyme, when coupled by a stiff power transmission to its external load, has to overcome a higher activation barrier than another enzyme with an elastically soft transmission. The softly coupled machine runs smoother and faster. Fig. 8, *bottom* illustrates this insight quantitatively. It gives the rate of rotation as function of the torsional rigidity of the power transmission. The steady-state drift velocity $\bar{V}$ in the periodic potential $\bar{U}(\theta)$ was calculated by solving the Smoluchowski equation (see Risken, 1996):

$$\bar{V} = \frac{\frac{2\pi}{3} k_B T (1 - e^{-2\pi T_1/3k_B T})}{\int_0^{2\pi/3} e^{U(\theta)/k_B T} d\theta \int_0^{2\pi/3} e^{-U(\theta)/k_B T} d\theta - (1 - e^{-2\pi T_1/3k_B T}) \cdot \int_0^{2\pi/3} e^{-U(\theta)/k_B T} \int_0^{\theta} e^{U(\theta')/k_B T} d\theta' \, d\theta} \quad (6)$$

It was apparent that the "kinetic efficiency" of the enzyme is greatly improved by a soft elastic power transmission. Another way to state this is to say that instead of having to wait for energy input by stochastic thermal collision to overcome the activation barrier, the elastically coupled enzyme could borrow elastic energy that had been transiently stored in the elastic power transmission during periods of downsliding the slopes of the original, more structured energy profile.

The arrow in Fig. 8, *bottom* indicates the assumed value of torsional rigidity of the γ subunit calculated for the elastic modulus of $2 \cdot 10^9$ $N \cdot m^{-2}$, which might serve as a rough estimate for the elasticity of F_1F_O transmission. At this elasticity and the enzyme torque of 56 pN · nm, the elastic deformation calculated by Eq. 2 is ~50°. The kinetic efficiency of an enzyme with such elastic parameters was analyzed in Cherepanov et al., 1999 and was found to be only twice lower than the maximal theoretical value. The comparable kinetic efficiency of 50% results also from the mechanical modeling presented in Fig. 8, *bottom*.

Was the observed elastic coupling attributable to the enzyme proper, or an artifact of its flexible attachment via his-tags and Ni-NTP-HRP to the surface of the solid support, and/or a soft **c**-ring/filament linkage? Although such flexible connections could smooth the filament dynamics, there are serious arguments against such effects.

First, a rather rigid biotin-streptactin linkage between F-actin and the **c**-ring was expected due to covalent attachments of several copies of the **c** subunit (which all carried an engineered strep-tag at their C-terminus) and the multi-biotinylated F-actin. The stiffness of the **c**-ring follows from the atomic force microscopy analysis (Seelert et al., 2000). A small compliance of the Ni-NTP-HRP–his-tags connection was expected if all three his-tags were involved in the attachment. The high surface concentration of bound HRP, forming a condensed protein monolayer on the glass interface, supported the saturation of the his-tag attachments.

Second, according to the data in Fig. 6, the fluctuation widths of rotating and nonrotating actin filaments of similar length were similar (almost identical after a slight correction for different length of the "free" end). As explained above, the blocked filaments were attached to at least two enzyme molecules in a row, such that the fluctuating free end was longer than the fixed strip between two attachment sites. Under these conditions, the angular compliance of the at-

tachment site and the **c**-ring/filament linkage matters for filaments that are attached to a single enzyme molecule only, and much less so for "immobilized" filaments which are attached to several enzyme molecules, say 500 nm apart from each other (the stiffness of the cross-beamed F-actin excludes effects of the angular compliance). Thus, the similar thermal mobility of rotating and nonrotating filaments provided a strong argument in favor of a rather rigid connection of the Ni-NTA-HRP–his-tag–F_OF_1–F-actin constructs.

Third, the used his-tags and biotin-streptactin loops probably did not possess a definite secondary structure. It was likely that they could not be elastically stretched under load. When uncoiled to the maximal extent, the hard covalent bonding restricted a further extension. Concerning the torque profile of F_1F_O in Fig. 7 *A*, a constant stretching of the linkages implied a certain phase shift, but not a smoothing of the output torque profile.

The concept of elastic power transmission is related to the "Stokes efficiency" of the enzyme as put forward by Wang and Oster (1998). Similar ideas were discussed elsewhere (Kinosita, Jr., et al., 2000a, b), where the time-resolved stepwise angular propagation of 1-μm-long filaments at an ATP concentration of 200 nM was reported. The data demonstrated that the stepwise displacement at 120° was essentially nonlinear: the motion could be approximated by a straight line in the middle part of the 120° interval (~60°), but was rather exponential at the ends. In other words, the data were useful to estimate the enzyme's torque in a narrow interval at the center of the 120° step (i.e., at three positions over 2π). Only the direct measurements of the torque at each point of the angular coordinate can clarify the situation. This task was solved in the present work.

SUMMARY AND CONCLUSIONS

ATP synthase produces ATP at the expense of ionmotive force. Under physiological conditions, in photosynthetic and respiring organisms, the torque that is generated by proton flow through the F_O motor operates against the counter-torque, which is generated by ATP hydrolysis in F_1. Under static head conditions, the two torques are eventually balanced, and the enzyme rests in a state of dynamic equilibrium. When operating close to this state, it may run very slowly under thermodynamic control. In this case, both the stator and the rotor portions are elastically strained. The situation is very different if one motor/generator is removed, then the remaining one runs freely under kinetic control. We studied the operation of an F_OF_1 construct in a situation very close to thermodynamic control. The torque was provided by ATP hydrolysis and the counter-torque was delivered to the **c**-ring of F_O by the elastic deformation of an attached actin filament that experienced viscous drag, friction, or obstacles. So far, our study related to a model system. Regrettably, the fully coupled enzyme, with protonmotive counter-torque, has so far withstood this approach for technical reasons.

In our hands, the common approach to estimate the average torque from the average rotation rate of the actin filaments and assuming that the filament felt the viscosity of the bulk medium yielded too low torque compared to the expected figure for a nonslipping rotary enzyme. This qualified previous conclusions as to a perfect, nonslipping operation between ATP hydrolysis in F_1 and torque generation (Wang and Oster, 1998; Kinosita, Jr., et al., 2000b). We showed in this article that the 5.6-nm-thick actin filament, which moved ~10 nm over ground, felt the (greater) surface viscosity, surface friction, and obstacles. This was apparent from 1) the rotation trajectories, 2) a correlation analysis of fluctuating and rotating filaments using the Langevin equation, and 3) experiments where the bulk viscosity was increased by adding sucrose.

This led us to an alternative approach: we gauged the torque by the elastic deformation of actin filaments. This technique was theoretically outlined elsewhere (Cherepanov and Junge, 2001). It was hardly sensitive to surface effects, but it required knowledge of the flexural rigidity of the actin filaments, which were used as a spring balance. Their rigidity was determined from bending thermal fluctuations, both of rotating and nonrotating filaments. The found figure for the flexural rigidity of F-actin, $8.2 \pm 3.0 \cdot 10^{-26}$ N · m^2, was consistent with the previously published findings based on the analysis of bending fluctuations of unconstrained filaments (Gittes et al., 1993; Isambert et al., 1995) and twisting fluctuations of immobilized and stretched F-actin filaments (Tsuda et al., 1996; Yasuda et al., 1996). Using our figures, we obtained an average torque of the F_OF_1 construct that was 1) three times greater than obtained by the common technique (Yasuda et al., 1998; Omote et al., 1999; Hisabori et al., 1999; Pänke et al., 2000), and 2) agreed reasonably well with the expected figure based on thermodynamic control in a perfectly coupled ATPase. The magnitude of the average torque, 50 ± 6 pN · nm, proved the absence of slip between ATP hydrolysis and torque production in F_1F_O-ATPase.

By using the curvature of elastically deformed and rotating filaments we calculated the torque profile of the F_1F_O molecule as function of the angular displacement. Precise measurements of the torque profile as function of the angular position are essential for understanding the role of the partial reactions (ATP binding, hydrolysis, product release) in torque generation. By using digital image analysis of long rotary trajectories and Fourier analysis we found a relatively smooth angular dependence of the torque that varied in the range of 30–80 pN · nm. The angular dependence had dominating periods of three and six over 2π, but their contributions in the Fourier spectrum were by one order of magnitude smaller than the extent of the constant component, and in some data sets hardly discernible from noise.

Integration of the output torque over the angular domain yielded the standard free energy. Its rather linear and featureless angular dependence was consistent with the concept of an elastic power transmission between the inner chemical motor in F_1 (the contact sites between subunits $(\alpha\beta)_3$ and γ) and the driving machinery of proton transfer (the ring of **c** subunits), which has been claimed as essential for the effective operation of the holoenzyme (Cherepanov et al., 1999; Pänke and Rumberg, 1999). An intrinsically stepping motor, when operating load-free and under kinetic control, runs up and down the valleys and hills of its free energy profile as illustrated by the solid line in Fig. 8, *top*. Its rate of progression depends on the Eyring-Polanyi (Arrhenius) argument on thermal input to cross the activation barrier. When such a motor is coupled to another one by an elastic power transmission, its output energy profile is flattened, broadly speaking, because of transient elastic storage of energy during the falling segments and utilization during the uprising segments of the energy profile of the motor proper. The elastic power transmission is considered as important 1) for the robust operation of this ubiquitous enzyme under symmetry mismatch (C_3 versus C_{10-14}), and 2) for high turnover rate of the two counteracting and stepping motor/generators in ATP synthase.

The authors thank H. Kenneweg and G. Hikade for excellent technical assistance.

This work was financially supported by grants from the Deutsche Forschungsgemeinschaft (SFB 431/D1, to W.J. and S.E.), the Human Science Frontier Program (RG 15/1998-M, to W.J.), the Fonds der chemischen Industrie and the Land Niedersachsen, and by an Alexander von Humboldt Fellowship (to D.C.).

O.P. and D.A.C. contributed equally to this work.

REFERENCES

Abrahams, J. P., A. G. W. Leslie, R. Lutter, and J. E. Walker. 1994. The structure of F_1-ATPase from bovine heart mitochondria determined at 2.8 Å resolution. *Nature.* 370:621–628.

Adachi, K., R. Yasuda, H. Noji, H. Itoh, Y. Harada, M. Yoshida, and K. Kinosita, Jr. 2000. Stepping rotation of F1-ATPase visualized through angle-resolved single-fluorophore imaging. *Proc. Natl. Acad. Sci. U.S.A.* 97:7243–7247.

Al-Shawi, M. K., C. J. Ketchum, and R. K. Nakamoto. 1997. Energy coupling, turnover, and stability of the FoF1 ATP synthase are dependent on the energy of interaction between gamma and β subunits. *J. Biol. Chem.* 272:2300–2306.

Althoff, G., H. Lill, and W. Junge. 1990. The single channel conductance of CF0. *In* Current Research in Photosynthesis, Proceedings of the VIII International Conference on Photosynthesis. 3:133–136. M. Baltscheffsky, editor. Kluwer, Dordrecht, the Netherlands.

Bevington, P. R. 1969. Data Reduction and Error Analysis for the Physical Sciences. McGraw-Hill, New York.

Boyer, P. D. 1997. The ATP synthase: a splendid molecular machine. *Annu. Rev. Biochem.* 66:717–749.

Cherepanov, D. A., and W. Junge. 2001. Viscoelastic dynamics of actin filaments coupled to rotary F-ATPase: curvature as an indicator of the torque. *Biophys. J.* 81:1234–1244.

Cherepanov, D. A., A. Mulkidjanian, and W. Junge. 1999. Transient accumulation of elastic energy in proton translocating ATP synthase. *FEBS Lett.* 449:1–6.

Dimroth, P. 2000. Operation of the F(0) motor of the ATP synthase. *Biochim. Biophys. Acta.* 1458:374–386.

Fasman, G. D. 1975. Handbook of Biochemistry and Molecular Biology. Physical and Chemical Data. CRC Press, Cleveland, Ohio.

Gittes, F., B. Mickey, J. Nettleton, and J. Howard. 1993. Flexural rigidity of microtubules and actin filaments measured from thermal fluctuations in shape. *J. Cell Biol.* 120:923–934.

Happel, J., and H. Brenner. 1983. Low Reynolds number hydrodynamics. Martinus Nijhoff Publishers, the Hague.

Häsler, K., S. Engelbrecht, and W. Junge. 1998. Three-stepped rotation of subunits γ and ε in single molecules of F-ATPase as revealed by polarized, confocal fluorometry. *FEBS Lett.* 426:301–304.

Hisabori, T., A. Kondoh, and M. Yoshida. 1999. The γ subunit in chloroplast F_1-ATPase can rotate in a unidirectional and counter-clockwise manner. *FEBS Lett.* 463:35–38.

Hunt, A. J., F. Gittes, and J. Howard. 1994. The force exerted by a single kinesin molecule against a viscous load. *Biophys. J.* 67:766–781.

Isambert, H., P. Venier, A. C. Maggs, A. Fattoum, R. Kassab, D. Pantaloni, and M. F. Carlier. 1995. Flexibility of actin filaments derived from thermal fluctuations. Effect of bound nucleotide, phalloidin, and muscle regulatory proteins. *J. Biol. Chem.* 270:11437–11444.

Jones, P. C., and R. H. Fillingame. 1998. Genetic fusions of subunit c in the F-0 sector of H+-transporting ATP synthase. Functional dimers and trimers and determination of stoichiometry by cross-linking analysis. *J. Biol. Chem.* 273:29701–29705.

Junge, W. 1999. ATP synthase and other motor proteins. *Proc. Natl. Acad. Sci. U.S.A.* 96:4735–4737.

Junge, W., H. Lill, and S. Engelbrecht. 1997. ATP synthase: an electrochemical transducer with rotatory mechanics. *TIBS.* 22:420–423.

Kinosita, K., Jr., R. Yasuda, and H. Noji. 2000a. F_1-ATPase: a highly efficient rotary ATP machine. *Essays Biochem.* 35:3–18.

Kinosita, K., Jr., R. Yasuda, H. Noji, and K. Adachi. 2000b. A rotary molecular motor that can work at near 100% efficiency. *Philos. Trans. R. Soc. Lond. B. Biol. Sci.* 355:473–489.

Kinosita, K., R. Yasuda, H. Noji, S. Ishiwata, and M. Yoshida. 1998. F_1-ATPase: a rotary motor made of a single molecule. *Cell.* 93:21–24.

Klionsky, D. J., W. S. A. Brusilow, and R. D. Simoni. 1984. In vivo evidence for the role of the epsilon subunit as an inhibitor of the proton-translocating ATPase of *Escherichia coli. J. Bacteriol.* 160: 1055–1060.

Krab, K., and J. Vanwezel. 1992. Improved derivation of phosphate potentials at different temperatures. *Biochim. Biophys. Acta.* 1098: 172–176.

Kuo, P. H., C. J. Ketchum, and R. K. Nakamoto. 1998. Stability and functionality of cysteineless F1F0 ATP synthase from *Escherichia coli. FEBS Lett.* 426:217–220.

Leslie, A. G., J. P. Abrahams, K. Braig, R. Lutter, R. I. Menz, G. L. Orriss, M. J. van Raaij, and J. E. Walker. 1999. The structure of bovine mitochondrial F1-ATPase: an example of rotary catalysis. *Biochem. Soc. Trans.* 27:37–42.

Leslie, A. G., and J. E. Walker. 2000. Structural model of F1-ATPase and the implications for rotary catalysis. *Philos. Trans. R. Soc. Lond. B. Biol. Sci.* 355:465–471.

Mendelson, R., and E. P. Morris. 1997. The structure of the acto-myosin subfragment 1 complex: results of searches using data from electron microscopy and x-ray crystallography. *Proc. Natl. Acad. Sci. U.S.A.* 94:8533–8538.

Noji, H., K. Häsler, W. Junge, K. Kinosita, Jr., M. Yoshida, and S. Engelbrecht. 1999. Rotation of *Escherichia coli* F(1)-ATPase. *Biochem. Biophys. Res. Commun.* 260:597–599.

Noji, H., R. Yasuda, M. Yoshida, and K. Kinosita. 1997. Direct observation of the rotation of F-ATPase. *Nature.* 386:299–302.

Omote, H., N. Sambonmatsu, K. Saito, Y. Sambongi, A. Iwamoto-Kihara, T. Yanagida, Y. Wada, and M. Futai. 1999. The γ subunit rotation and

torque generation in F_1-ATPase from wild-type or uncoupled mutant *Escherichia coli*. *Proc. Natl. Acad. Sci. U.S.A.* 96:7780–7784.

Oster, G., and H. Wang. 1999. ATP synthase: two motors, two fuels. *Structure.* 7:R67–R72.

Pänke, O., K. Gumbiowski, W. Junge, and S. Engelbrecht. 2000. F-ATPase: specific observation of the rotating c-subunit oligomer of EF_OEF_1. *FEBS Lett.* 472:34–38.

Pänke, O., and B. Rumberg. 1997. Energy and entropy balance of ATP synthesis. *Biochim. Biophys. Acta.* 1322:183–194.

Pänke, O., and B. Rumberg. 1999. Kinetic modeling of rotary CF_0F_1-ATP synthase: storage of elastic energy during energy transduction. *Biochim. Biophys. Acta.* 1412:118–128.

Pardee, J. D., and J. A. Spudich. 1982. Purification of muscle actin. *Methods Enzymol.* 85:164–170.

Risken, H. 1996. The Fokker-Planck equation. Methods of solution and applications. Springer-Verlag, Berlin.

Sabbert, D., S. Engelbrecht, and W. Junge. 1997. Functional and idling rotatory motion within F-ATPase. *Proc. Natl. Acad. Sci. U.S.A.* 94: 4401–4405.

Sabbert, D., and W. Junge. 1997. Stepped versus continuous rotatory motors at the molecular scale. *Proc. Natl. Acad. Sci. U.S.A.* 94: 2312–2317.

Sambongi, Y., Y. Iko, M. Tanabe, H. Omote, A. Iwamoto-Kihara, I. Ueda, T. Yanagida, Y. Wada, and M. Futai. 1999. Mechanical rotation of the c subunit oligomer in ATP synthase (FoF1): direct observation. *Science.* 286:1722–1724.

Sedmak, J. J., and S. E. Grossberg. 1994. A rapid, sensitive, and versatile assay for protein using Coomassie brilliant blue G250. *Anal. Biochem.* 79:544–552.

Seelert, H., A. Poetsch, N. A. Dencher, A. Engel, H. Stahlberg, and D. J. Mueller. 2000. Proton-powered turbine of a plant motor. *Nature.* 405: 418–419.

Stahlberg, H., D. J. Müller, K. Suda, D. Fotiadis, A. Engel, T. Meier, U. Matthey, and P. Dimroth. 2001. Bacterial Na^+-ATP synthase has an undecameric rotor. *EMBO Reports*. 2:229–233.

Stock, D., A. G. Leslie, and J. E. Walker. 1999. Molecular architecture of the rotary motor in ATP synthase. *Science.* 286:1700–1705.

Syroeshkin, A. V., L. E. Bakeeva, and D. A. Cherepanov. 1998. Contraction transitions of F1–F0 ATPase during catalytic turnover. *Biochim. Biophys. Acta.* 1409:59–71.

Tsuda, Y., H. Yasutake, A. Ishijima, and T. Yanagida. 1996. Torsional rigidity of single actin filaments and actin-actin bond breaking force under torsion measured directly by in vitro micromanipulation. *Proc. Natl. Acad. Sci. U.S.A.* 93:12937–12942.

Tsunoda, S. P., R. Aggeler, H. Noji, K. Kinosita, M. Yoshida, and R. A. Capaldi. 2000. Observations of rotation within the F_OF_1-ATP synthase: deciding between rotation of the F(o)c subunit ring and artifact. *FEBS Lett.* 470:244–248.

Wang, H. Y., and G. Oster. 1998. Energy transduction in the F-1 motor of ATP synthase. *Nature.* 396:279–282.

Weber, J., and A. E. Senior. 1996. Binding and hydrolysis of TNP-ATP by *Escherichia coli* F_1-ATPase. *J. Biol. Chem.* 271:3474–3477.

Wise, J. G. 1990. Site-directed mutagenesis of the conserved beta subunit tyrosine 331 of *Escherichia coli* ATP synthase yields catalytically active enzymes. *J. Biol. Chem.* 265:10403–10409.

Xu, J., W. H. Schwarz, J. A. Käs, T. P. Stossel, P. A. Janmey, and T. D. Pollard. 1998. Mechanical properties of actin filament networks depend on preparation, polymerization conditions, and storage of actin monomers. *Biophys. J.* 74:2731–2740.

Yanagida, T., M. Nakase, K. Nishiyama, and F. Oosawa. 1984. Direct observation of motion of single F-actin filaments in the presence of myosin. *Nature.* 307:58–60.

Yasuda, R., H. Miyata, and K. Kinosita, Jr. 1996. Direct measurement of the torsional rigidity of single actin filaments. *J. Mol. Biol.* 263:227–236.

Yasuda, R., H. Noji, K. Kinosita, and M. Yoshida. 1998. F_1-ATPase is a highly efficient molecular motor that rotates with discrete 120° steps. *Cell.* 93:1117–1124.

Yasuda, R., H. Noji, M. Yoshida, K. Kinosita, Jr., and H. Itoh. 2001. Resolution of distinct rotational substeps by submillisecond kinetic analysis of F1-ATPase. *Nature.* 410:898–904.